The origin of the large bending enhancement of the reaction of $C_2H_2^+$ with methane: the effects of bending momentum, ruling out the precursor mechanism, and steps toward "Polanyi rules" for polyatomic reactions†

Jianbo Liu*[a] and Scott L. Anderson[b]

Received 27th April 2009, Accepted 23rd June 2009
First published as an Advance Article on the web 28th July 2009
DOI: 10.1039/b908328f

Quasi-classical trajectories for the hydrogen abstraction (HA) reaction $C_2H_2^+ + CH_4 \rightarrow C_2H_3^+ + CH_3$, were analyzed to probe the mechanistic origins of the large, mode-specific reactivity enhancement observed experimentally following excitation of the $C_2H_2^+$ *cis*-bending mode. The trajectories show the correct trend in reactivity *vs.* CC stretch and bending excitations, and also reproduce the experimental recoil velocity map. Analysis of the trajectories shows that at collision energy of 0.5 eV hydrogen abstraction is dominated by a direct mechanism, but ~15% of the reaction is mediated by a precursor complex. The vibrational enhancement mostly comes from direct collisions. The bending vibration enhances the reactivity in two ways. Collisions in bent geometries (of $C_2H_2^+$) are more reactive; however, the dominant vibrational effect is a consequence of the momentum associated with the bending vibration. Enhancement by vibrational momentum is reminiscent of the behavior seen by Polanyi and co-workers for late barrier A + BC reactions, and indeed, the atom transfer event in the $C_2H_2^+ + CH_4$ system does occur late in the collision. We, therefore, explore the possibilities for interpreting polyatomic vibrational dynamics in a "Polanyi Rule" context, using trajectories to guide the construction of a reduced dimensionality surface.

I. Introduction

The reaction of $C_2H_2^+$ with methane has been the subject of a number of experimental and theoretical studies.[1–14] In particular, Chiu *et al.* reported the effects of collision energy and $C_2H_2^+$ vibrational excitation on reactivity and product recoil dynamics, providing a stringent benchmark for mechanism development.[12] Both total reactivity and branching to the endoergic hydrogen abstraction channel were found to be strongly and mode-specifically enhanced by excitation of the $C_2H_2^+$ *cis*-bending vibration. Collision energy and CC stretch excitation had much smaller, and in some cases, inhibitory effects. The main goal of this study is to unravel the origin of the large bending vibrational enhancement.

Klippenstein[13] proposed a model to rationalize the vibrational effects within a transition state theory framework. The model assumes that reaction at low energies is mediated by a weakly-bound, precursor complex, which is indeed a feature of the calculated potential energy surface (*vide infra*). To introduce mode-specificity, it was proposed that some modes do not couple to the ergodic bath states available to drive decomposition of the complex. The experimental data of recoil behavior does provide indirect evidence that such a complex might play a role at low energies, but there is no direct evidence of the importance of this mechanism. Because of strong ion-induced-dipole forces, many ion–molecule systems have shallow, reactant-like wells on their potential energy surfaces, thus precursor complexes almost certainly play a role in reaction at low collision energies. We have seen evidence suggesting mediation by precursor complexes in many reactions, and in some there is also mode-specific reactivity in the energy range where the precursor appears to be significant. Indeed, we proposed a variation on the selective coupling idea to account for mode-specific reaction of $C_6H_5OH^+$ with ND_3.[15] A subsidiary purpose of the present study is to look for evidence of precursor complex effects on the scattering mechanism and vibrational enhancement.

We carried out a detailed quasi-classical trajectory (QCT) simulation of $C_2H_2^+ + CH_4$ collisions at 0.5 eV collision energy, focusing on the hydrogen abstraction (HA) reaction $C_2H_2^+ + CH_4 \rightarrow C_2H_3^+ + CH_3$, which is both the major channel at this energy, and the channel with the largest vibrational mode effects. Before describing the trajectory methodology and results, we first outline the key features of the reaction coordinate and previous experimental results.

II. Summary of the reaction coordinate and experimental results

The reaction of $C_2H_2^+$ with CH_4 has the following channels observed at low collision energies. The energetics are derived

[a] *Department of Chemistry and Biochemistry, Queens College and the Graduate Center of the City University of New York, 65-30 Kissena Blvd., Flushing, New York 11367, USA. E-mail: jianbo.liu@qc.cuny.edu*
[b] *Department of Chemistry, University of Utah, 315 S. 1400 E. Rm, 2020, Salt Lake City, Utah 84112, USA*

† Electronic supplementary information (ESI) available: Videos showing non-reactive and reactive trajectories. See DOI: 10.1039/b908328f

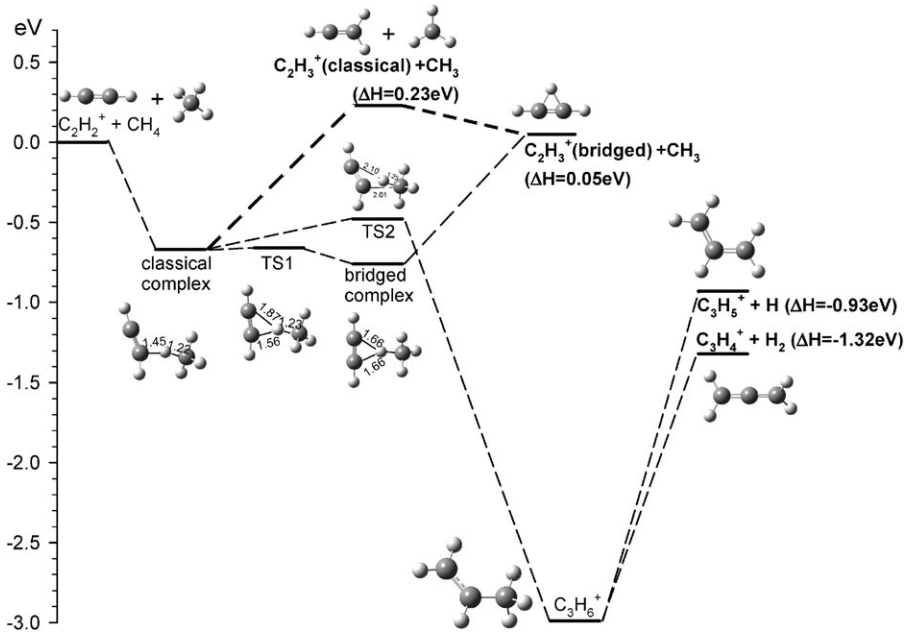

Fig. 1 Schematic reaction coordinate for $C_2H_2^+ + CH_4$. Energies are derived from a combination of experimental, G3(298 K) and MP2/6-31+G* (298 K) values.

from a combination of experimental,[16,17] G3(298 K) and MP2/6-31+G**(298 K) values:

$$C_2H_2^+ + CH_4 \rightarrow C_2H_3^+ \text{ (bridged)} + CH_3 \text{ (hydrogen abstraction = HA)} \quad \Delta_r H^\circ = 0.05 \text{ eV}$$

$$C_2H_2^+ + CH_4 \rightarrow C_2H_3^+ \text{ (classical)} + CH_3 \text{ (HA)} \; \Delta_r H^\circ = 0.23 \text{ eV}$$

$$C_2H_2^+ + CH_4 \rightarrow C_3H_4^+ + H_2 \; (H_2 \text{ elimination}) \; \Delta_r H^\circ = -1.32 \text{ eV}$$

$$C_2H_2^+ + CH_4 \rightarrow C_3H_5^+ + H \; (H \text{ elimination}) \; \Delta_r H^\circ = -0.93 \text{ eV}$$

An *ab initio* reaction coordinate for this system is shown in Fig. 1. The structures of stationary points and transition states were calculated at B3PW91/6-31+G*, B3LYP/6-31+G*, MP2/6-31+G** and G3 levels of theory. The results are in good agreement with previous calculations.[13,14] The main points of the reaction coordinate are as follows: (1) reactant-like precursor complexes of both classical and bridged geometries are bound by 0.6–0.8 eV with respect to both reactants and HA products, but by only 0.2–0.3 eV with respect to TS2, leading to a covalently bound $C_3H_6^+$ complex. Because the precursor complexes have geometries similar to reactants, it is unlikely that there would be significant activation barriers to forming them; (2) dissociation of the precursors to the corresponding HA products is barrierless; (3) the bridged form of both precursor complex and HA products is more stable than the corresponding classical geometry; however, the classical form might be expected to dominate because it can form in a wider range of geometries. Interconversion between classical and bridged structures should be possible; (4) TS2, leading to the covalently bound $C_3H_6^+$ complex, is relatively tight compared to the orbiting TSs[18] leading back to reactants or to HA products, thus the covalent $C_3H_6^+$ complex, and the $C_3H_{6-x}^+$ channels depending on it, should become unimportant at high collision energies, as was observed experimentally. Furthermore, while the covalent $C_3H_6^+$ complex can contribute to HA by CH_3–loss, H or H_2 elimination should be more facile, and the contribution of the covalent complex to the HA channel is expected to be small, except at very low energies. This conclusion was verified with isotope labeling in the experimental study.[12]

Properties such as vibrational state or collision energy effects on reactivity can only depend on dynamics leading up to the rate-limiting step on the reaction coordinate,[19–22] and because of the strong mode dependence it is clear that the rate-limiting step occurs early in $C_2H_2^+ + CH_4$ collisions, before the initial mode of vibrational excitation has been randomized. Product recoil behavior, of course, depends on dynamics throughout the course of the collisions, however, the gross features of the scattering (stripping *vs.* rebound dynamics, energy disposal) may still reflect events that occur early in the collisions. Such reactions are ideal for quasi-classical trajectory study because error tends to accumulate during a trajectory.[23]

The experimental integral cross-sections relevant to this study are summarized in Fig. 2 as a function of the center-of-mass collision energy E_{col}, for $C_2H_2^+$ in its ground state, and with excitation in the CC stretch (ν_2^+), and *cis*-bending overtone ($2\nu_5^+$).[12] As indicated in Fig. 1, the $C_3H_5^+ + H$ and $C_3H_4^+ + H_2$ channels both result from decay of the covalent $C_3H_6^+$ complex, and have nearly identical dynamics. Therefore we give only the cross section for the sum of the two: $C_3H_{6-x}^+ + H_x$, $x = 1$ and 2. The HA reaction shows enhancement by collision energy at low E_{col}, as expected for an endoergic reaction, but by $\sim$0.5 eV, collision energy begins to inhibit HA, albeit weakly. Both channels, but especially the HA channel, are enhanced strongly by

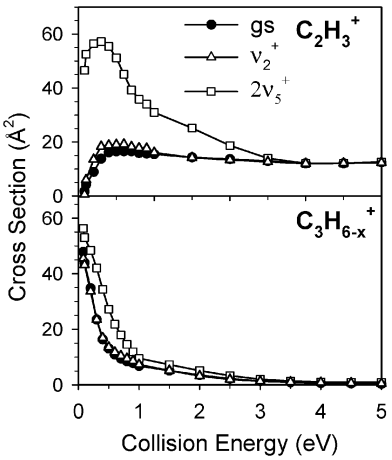

Fig. 2 Reaction cross sections for ground state and vibrational excited $C_2H_2^+$ with methane.

$C_2H_2^+$ *cis*-bending excitation ($2\nu_5^+$ 155 meV) at low E_{col}. In contrast, excitation of the CC stretch mode (ν_2^+ 225 meV) has little effect on either channel.

Note that there are two obvious mechanistic regimes. For collision energies above 2 eV there is little E_{col} or vibrational state dependence, and recoil velocity measurements show that the reaction is dominated by a direct, stripping mechanism. In this "high energy" regime, the $C_3H_{6-x}^+$ products, which require a complex to mediate the needed rearrangements, are minor channels. At E_{col} below $\sim$1 eV, both vibrational and E_{col} effects are large and the $C_3H_{6-x}^+$ channels become increasingly important. The recoil velocity measurements are consistent with, but do not prove mediation of this "low energy" mechanism by a precursor complex, as proposed in the experimental paper and by Klippenstein. The calculations described below were carried out at a collision energy of 0.5 eV—just in the middle of the "low energy" mechanistic range, where vibrationally mode-specific enhancement is at its maximum.

III. Computational details

Quasi-classical, direct dynamics trajectories were calculated using the general chemical dynamics program VENUS99 of Hase *et al.*[24] to set up the trajectory initial conditions, and the Hessian-based method of Bakken *et al.*[25] implemented in Gaussian 03(revision C.01),[26] to propagate each trajectory, with Hessians recalculated every five steps. The integrations were performed with a step size of 0.25 amu$^{1/2}$ a_0 ($\sim$0.7 fs), which conserved total energy to better than 10^{-4} Hartree. The SCF = XQC option was used during trajectory integration so that a quadratically convergent Hartree–Fock (QC-SCF) method[26,27] was used in case the usual, but much faster, first-order SCF method did not converge within the allotted number of cycles.

Because millions of gradients and Hessian evaluations were required, the level of *ab initio* theory used was necessarily modest. To select a suitable level of theory, we calculated several reactive and non-reactive trajectories at the MP2/6-31+G* and B3LYP/6-31+G* levels of theory, and for each trajectory we selected seven geometries corresponding to chemically important steps in the collision: reactants, products, points where bonds appear to be breaking or forming in various orientations. The energies for these selected geometries were then calculated at candidate levels of theory (including MP2/6-31+G*, MP2/6-311++G**, B3LYP/6-31+G*, B3LYP/6-311++G**, B3PW91/6-31+G* and B3PW91/6-311++G**), and compared to CCSD/cc-pVTZ and QCISD(T)/cc-pVTZ energies. On the basis of the overall level of agreement and computational speed, we chose the MP2/6-31+G* level of theory for the main set of trajectories. The MP2/6-31+G* endoergicity of the HA reaction is slightly greater than the experimental or G3 values [0.13 eV at MP2 *vs.* 0.05 eV[16] for $C_2H_3^+$ (bridged) + CH_3, and 0.33 eV at MP2 eV *vs.* 0.23 eV at G3 for $C_2H_3^+$ (classical) + CH_3]. These errors appear to be a problem with both MP2 and B3LYP methods, and the B3LYP/6-31+G* error is even worse. As a result, we expect that the absolute value of the reaction cross section calculated from the trajectory results is likely to be lower than the experimental value. There is reason to hope that the calculated vibrational enhancement should be reasonable, however, because the MP2 energetics for reactant approach and the various barriers on the early part of the reaction coordinate are more accurate.

The initial conditions for the trajectories were chosen to mimic the conditions of the experimental study of Chiu *et al.*[12] Because in the experiment the $C_2H_2^+$ ions were generated by photoionization of a supersonic molecular beam, a 50 K Boltzmann distribution was sampled to select the $C_2H_2^+$ initial rotational state. The CH_4 in the experiments was at room temperature, so a rotational temperature of 300 K was used. The quasi-classical initial vibrational state is simulated by giving each reactant atom displacement from equilibrium and momentum appropriate to the desired initial rovibrational state, with random phases for the different modes. The trajectories were run with both $C_2H_2^+$ and CH_4 having zero-point energy (ZPE, total 1.86 eV at MP2/6-31+G*) in all vibrational modes, and with $C_2H_2^+$ either in its ground state or having two additional quanta of excitation in ν_5^+ (184 meV for $2\nu_5^+$ at MP2/6-31+G*). To test the mode dependence of vibrational effects, we also ran a set of trajectories with excitation of the ν_2^+ mode (230 meV at MP2/6-31+G*) of $C_2H_2^+$. For this set, intended only as a check that the mode dependence is correct, we only calculated trajectories for the range of the impact parameters that make significant contributions to the reactivity. Trajectories were calculated for only one collision energy, 0.5 eV; chosen for several reasons. The vibrational effects are still large at this energy, and both the experimental cross sections and the recoil angular data suggest that the mechanism is still in the "low energy" regime where precursor mediation may play a role in the vibrational mode specificity. Because precursor lifetime should increase rapidly with decreasing energy, it was felt that collisions at lower E_{col} might have collision times too long for practical trajectory simulations.

Because the number of trajectories was necessarily limited, we adopted a previously successful strategy[23,28] to minimize statistical error in comparing behavior for different $C_2H_2^+$ states or impact parameters. For each state, batches of trajectories (typically 100) were calculated for discrete values

of the reactant impact parameter rather than randomly sampling the b distribution. For both the ground and $2\nu_5^+$ states, trajectories were run at ten discrete values of the impact parameter, ranging from 0.1 to 5.0 Å, allowing us to examine the b dependence of the scattering dynamics in detail. For the ν_2^+ state, trajectories were calculated at four different values of the impact parameter (b = 1.0, 2.0, 3.0 and 4.0 Å). Collisions at impact parameters below 1.0 Å were omitted because their weighting in the integral cross section is small, and only 50 trajectories were calculated at b = 4.0 Å because no reaction was observed.

The random number generator seed used in setting up initial conditions for each batch of trajectories was identical. Each trajectory batch, therefore, used the same pseudo-random sequence to sample the reactant parameters (orientations, rotational energies, rotational and vibrational phases, *etc.*). As a result, it is easy to compare trajectories for different $C_2H_2^+$ vibrational states or impact parameters, because corresponding trajectories from different batches have identical initial conditions, apart from the parameter being varied (*i.e.*, the $C_2H_2^+$ vibrational state or impact parameter). The main motivation for this pseudo-random sampling procedure was to avoid a potentially serious problem that arises when reactivity is sharply dependent on one or more reactant parameters. By using the same pseudo-random sequence for each batch, the error from inadequate sampling of reactant parameter space is the same for all batches, and tends to cancel when comparing batches for different states or impact parameters.

All trajectories started with an initial center-of-mass reactant separation of 6.0 Å, and were terminated either when the distance between the final products exceeded 9.0 Å, or after 2000 steps. This relatively short separation was used to insure that the initial state did not have time to decay by anharmonic coupling during the reactant approach. The error in the energy due to the long-range potential at 6 Å is negligible (less than 5 meV). About 2350 trajectories were calculated, each taking $\sim$24 CPU h on Athlon 64-based cluster. For trajectory visualization we used the program gOpenMol.[29] Detailed analysis of individual trajectories and statistical analysis of the trajectory ensemble were done with programs written for this purpose,[30–33] available from the corresponding author upon request.

There are two issues with using the QCT method to probe vibrational dynamics. One obvious point is that vibration energy is not quantized, leading to several types of non-physical behavior. At the start of the trajectories, the vibrational energy is partitioned appropriately to represent the classical analog of the desired initial quantum state. During the time required for reactant approach, the initial energy partitioning can decay *via* anharmonic coupling of the normal modes, such that the vibrational motion at the moment of collision no longer represents the state of interest. We started the trajectories with reactant center-of-mass separation of only 6.0 Å, so that only $\sim$100 fs elapses prior to the collision. In addition, because both reactants are small molecules, the number of symmetry-allowed mode combinations capable of coupling to the initial state is limited. We examined the $C_2H_2^+$ vibrational motion over a time scale much longer than the reactant approach time and found no significant changes in the character of the vibrational motion (*i.e.*, maximum bending angle, and maximum and minimum CH bond lengths). Therefore, at the "moment of collision", the trajectories still represent the desired states, at least to the extent possible in the quasi-classical framework. Lack of quantization presumably has a significant effect on how energy is distributed between vibrational modes during and after collisions.[34,35] It is possible to have trajectories where final E'_{vib} is below the zero point level. Such unphysical collisions were found to be negligible in our trajectories, presumably because we are looking at relatively high energy collisions, reducing the error associated with treating the motion classically. More importantly, the observables of greatest interest for our purposes are the effects of the different $C_2H_2^+$ vibrational modes on the HA cross section, which depend only on dynamics up to the rate-limiting point on the reaction coordinate. The experimental observation of strong, mode-specific vibrational effects indicates that the rate-limiting point must be early in the collision, before the initial excitation is scrambled. Such system is ideal for QCT.

IV. Trajectory results and discussion

A Nature of the trajectories

Roughly 77.8% of all trajectories are characterized as direct, nonreactive scattering, resulting in conversion of some collision energy into vibrational and rotational energy ($T \rightarrow E_{internal}$ conversion). The remaining trajectories either formed HA products ($C_2H_3^+ + CH_3$, 17.6%) or $C_3H_{6-x}^+$ products ($C_3H_6^+$, $C_3H_5^+ + H$, and $C_3H_4^+ + H_2$, total 4.6%). In most HA trajectories, the $C_2H_3^+$ product ions are produced initially in the classical structure, sometimes isomerizing to the bridge structure before trajectory termination. The $C_3H_6^+$ "product" simply represents complexes that would dissociate, almost entirely by H or H_2 elimination, if the trajectories were allowed to propagate long enough.

A typical HA trajectory is illustrated in Fig. 3, showing changes of various distances and the potential energy (PE) during the trajectory. The CM distance is the distance between the centers of mass of the collision partners, and the two CH bond lengths plotted correspond to the H_3C–H bond being broken, and the H–C_2H_2 bond being formed in the reaction. The oscillations in the bond lengths and PE reflect the vibrations of the reactants or products, including ZPE. The HA trajectory is direct, with only one turning point in the relative motion of the reactant centers of mass, *i.e.*, there is no sign of mediation by a complex in this collision. The time for reactant approach is around 100 fs, and the time during which the interaction is strong is $\sim$50 fs, which is comparable to the periods of the lower-frequency $C_2H_2^+$ vibrations. We note that the actual hydrogen abstraction event, defined as the time point where the CH bond of methane first extends by more than 2 times the amplitude of the ZPE, occurs $\sim$40 fs after the CM turning point, *i.e.*, reaction occurs late, as the collision partners rebound.

B Trajectory validation

Before analyzing what the trajectories tells us about the dynamics, it is important to verify that the trajectories are in

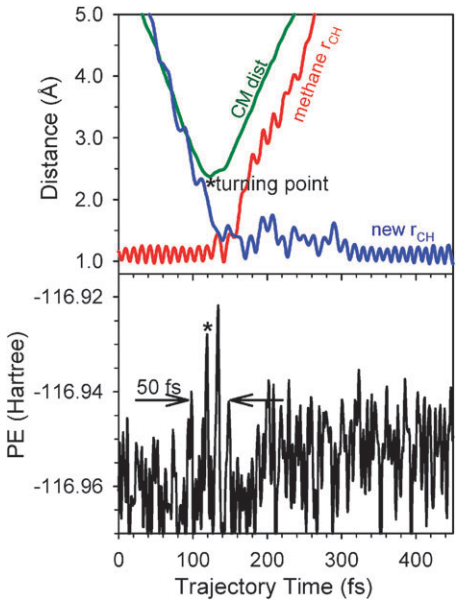

Fig. 3 A representative plot of hydrogen abstraction trajectories. (Top) The variation of various bond lengths and center-of-mass separation during the trajectory, and (bottom) the variation of potential energy during the trajectory.

reasonable agreement with experiment. We start by comparing trajectory HA reaction cross sections with those from the experiment. Because trajectories were calculated at discrete b values, the trajectory cross sections were estimated using an extended closed trapezoidal approximation[36] to the usual integral form (eqn (1)), where $P(b)$ is the fraction of reactive trajectories at each impact parameter, *i.e.*, the opacity function:

$$\sigma = 2\pi \int_0^{b_{max}} P(b) b db$$

$$\approx \pi \sum_{b_i=0}^{b_{max}} [P(b_i) \times b_i + P(b_{i+1}) \times b_{i+1}] \times (b_{i+1} - b_i)$$

The maximum b at which reaction is observed is 3.5 Å for all vibrational states. Table 1 compares the calculated HA cross sections to those measured in the experiment.[12] The error limits given for the trajectory cross section are statistical, based on the number of total trajectories and reactive trajectories for each initial condition, and obviously do not include any systematic errors. The absolute cross sections from the trajectory results are systematically smaller than the experimental cross sections. We attribute the lowered reactivity mostly to the fact, discussed above, that the endoergicity of the HA reaction calculated at the MP2/6-31+G* level used in the trajectories, is ~100 meV too high, although other inaccuracies in the QCT method may also contribute. The more important results are the relative cross sections, *i.e.*, the effects of ν_2^+ and $2\nu_5^+$ excitation. Experimentally at $E_{col} = 0.5$ eV, the enhancement factor ($\sigma(\nu^+)/\sigma(gs)$) is 1.2 for the ν_2^+ state, and 2.6 for $2\nu_5^+$. The trajectories show the correct trend for the two excited states, with strong mode specificity favoring the bending excitation. The trajectory calculated vibrational enhancement factors are 1.16 and 1.55 for the ν_2^+ and $2\nu_5^+$ states, respectively. The $2\nu_5^+$ enhancement is a factor of 1.7 higher than that of ν_2^+ *per* unit energy. Note that the trajectory calculated enhancement factors are smaller compared to the experimental values. This "damping" of the vibrational effects is typical in our experience with QCT studies of vibrational effects[23,28,30–32] and we tentatively associate it with the failure to quantize vibrational motion. Nonetheless, the results suggest that the trajectories capture the physics of the mode-specific vibrational enhancement, at least qualitatively.

The other experimental observation that the trajectories can be tested against is the product recoil velocity distributions. Table 1 presents the experimental and calculated mean recoil energy $\langle E_{recoil} \rangle$, the fraction of E_{avail} going into recoil ($\langle E_{recoil} \rangle / \langle E_{avail} \rangle$, $E_{avail} = E_{col} + E_{vib} + E_{rot} - \Delta H$) and the scattering angle $\langle \theta_{scat} \rangle$, for reactions with $C_2H_2^+$ in three different states. Note that the "uncertainties" shown for $\langle E_{recoil} \rangle$ and $\langle \theta_{scat} \rangle$ are actually the widths (at half-maximum) of the recoil energy and scattering angle distributions. The average and widths of the recoil energy distributions are in excellent agreement with the values estimated from the experiments.[12] In both experiment and trajectories, excitation of ν_2^+ or $2\nu_5^+$ leads to a decreased fraction of available energy (E_{avail}) going into recoil.

Fig. 4 reports the 2-D $C_2H_3^+$ recoil velocity map from the trajectories for ground state $C_2H_2^+$. The peak contribution for each trajectory set at different impact parameters is indicated by the superimposed numbers, and the map is simply the $P(b) \times b$-weighted sum of the product ion recoil distributions obtained for each set. There clearly is a strong correlation between the impact parameter and the scattering angle, with small b leading to rebounding, and large b leading to stripping, as expected for a direct collision mechanism.[20,31] The one-to-one mapping of b to scattering angle shows that the dominant mechanism at this energy is direct, however, as shown below, there is significant fraction of trajectories with collisions times ranging up to >1000 fs, *i.e.*, collisions mediated by complexes with lifetimes comparable to the rotational period. These complex-mediated collisions give recoil angular distributions

Table 1 Comparison of trajectory and experimental results for the HA reaction at $E_{col} = 0.5$ eV

	Experiment				Trajectory				
	σ_{HA}/Å^2	$\langle E_{recoil} \rangle^a$/eV	$\langle E_{recoil} \rangle / \langle E_{avail} \rangle^a$	$\sigma(\nu^+)/\sigma$/gs	σ_{HA}/Å^2	$\langle E_{recoil} \rangle$/eV	$\langle E_{recoil} \rangle / \langle E_{avail} \rangle$	$\langle \theta_{scatl} \rangle$/°	$\sigma(\nu^+)/\sigma$/gs
gs	16	0.22 ± 0.12	0.49	—	8.1 ± 0.9	0.23 ± 0.11	0.55	55 ± 29	—
ν_2^+	20	0.24 ± 0.15	0.32	1.2	9.4 ± 0.7	0.27 ± 0.11	0.42	57 ± 30	1.16
$2\nu_5^+$	42	0.24 ± 0.14	0.40	2.6	12.6 ± 1.1	0.26 ± 0.12	0.43	50 ± 21	1.55

[a] Values are estimated from experimental measurements taken at $E_{col} = 0.4$ and 0.8 eV.[12]

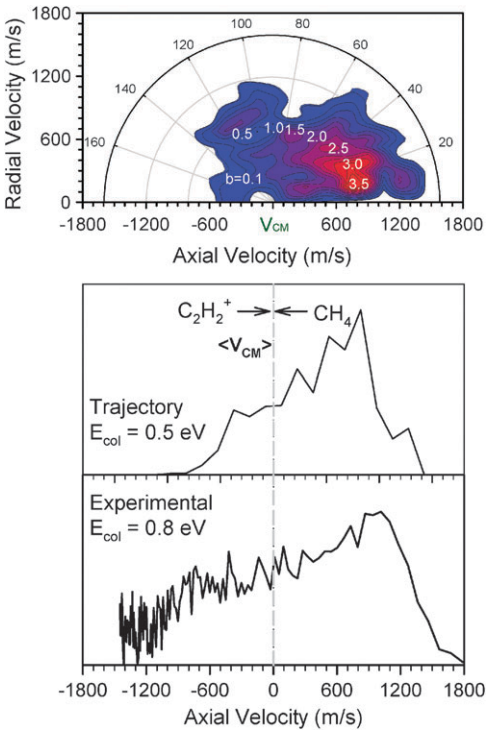

Fig. 4 (Top) Computed 2-D $C_2H_3^+$ velocity contour map, and (bottom) comparison of computed $C_2H_3^+$ axial velocity distribution at E_{col} of 0.5 eV and experimental measured $C_2H_3^+$ axial velocity distribution at nominal E_{col} of 0.8 eV. The numbers on the map show the most probable recoil velocity for each value of reactant b.

that contribute to a broad background that underlies the b-to-θ mapping from the direct collisions.

In the experimental paper[12] only the v_{axial} distributions (*i.e.*, projection of the full 2-D recoil velocity distributions on the axis of the instrument) were reported. In the experimental arrangement the instrument axis is coincident (on average) with $v_{relative}$, *i.e.*, the relative velocity of the collisions. To allow comparison, the lower half of the figure compares an experimental v_{axial} distribution (unfortunately for a somewhat higher E_{col}) with the projection of the trajectory velocity map onto $v_{relative}$, which is essentially what the experiment measures, albeit with broadening from the ion beam and neutral velocity distributions. As expected from the higher available energy in the experiment, the peak and width of the recoil velocity distribution is larger than in the trajectories, however the shapes are quite similar. Both distributions are asymmetric and forward scattered with respect to the origin of the center-of-mass frame, indicating that reaction is dominated by a direct mechanism. In both trajectories and experiments, however, the angular distributions are broad, and the experimental recoil distributions were best fit by a combination of direct and complex-mediated mechanisms, with the direct mechanism becoming dominant with increasing collision energy. This combination of direct and complex-mediated mechanisms is quite consistent with the trajectory results.

We also compared the experimental and calculated v_{axial} distributions for reaction of $C_2H_2^+$ in its ν_2^+ and $2\nu_5^+$ states. These are not shown, as they are quite similar to those for the ground state reactants, except that vibrational excitation slightly increases $\langle E_{recoil} \rangle$, and excitation of $2\nu_5^+$ also increases the degree of forward peaking as indicated in Table 1. The weak dependence of recoil velocity on reactant vibrational state is typical for most ion–molecule reactions,[19,37,38] reflecting the fact that recoil is largely controlled by kinematics, available energy, and exit channel interactions, none of which is much affected by modest vibrational excitation.

Overall, the trajectory results are in excellent agreement with experiment, considering the limitations of the QCT method. Therefore, we feel confident in examining the trajectories in more detail in order to extract additional mechanistic insight. Since both experimental and trajectory results show weak enhancement by the ν_2^+ CC stretch excitation, we will mostly focus on the dynamics of $2\nu_5^+$ bending excitation in the following discussion.

C HA reaction dynamics

1 Dependence on impact parameter. From eqn (1), it can be seen that the magnitude of HA cross section is determined by how the opacity function, $P(b)$, varies with b. The increase in cross section with $2\nu_5^+$ excitation could result from increase in the magnitude of $P(b)$, or an increase in the range b over which $P(b)$ is significant, or both. The trajectory opacity functions are given in Fig. 5. Also shown in Fig. 5 are b-weighted opacity functions $P(b) \times b$'s (*i.e.*, the contribution of each range of b to the reaction cross section) and the cross section enhancement due to the $2\nu_5^+$ excitation (shaded area). Within the uncertainty, the vibrational enhancement is the result of a uniform increase in reaction probability across the entire range of reactive impact parameters, and the range is not extended. $P(b)$ is nearly constant up to a maximum b, beyond which no reaction is observed. This b_{max} is identical (3.5 Å) for $C_2H_2^+$ in its ground state and two excited states, and is slightly smaller than the orientation-averaged hard-sphere collision radius of ~4.0 Å. Because the cross section scales like $P(b) \times b$, the consequence is that the major contribution to

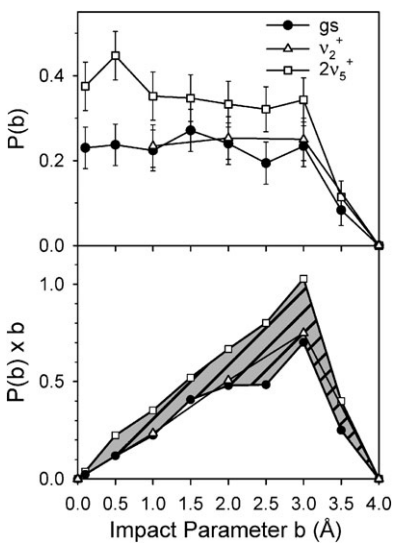

Fig. 5 HA opacity functions for different vibrational states. The vibrational enhancement by $2\nu_5^+$ excitation is indicated by the shaded area.

the cross section for all three states comes from collisions with b between 2.0 and 3.5 Å. This behavior is essentially the opposite of what would be expected in a line-of-centers (LOC) picture,[39] where the magnitude of $P(b)$ should be the same for different vibrational states, but the range of reactive impact parameters should increase with vibrational excitation because less $T \rightarrow E_{internal}$ conversion is required to drive reaction.

We also investigated partitioning of available energy into the products of the HA reaction. Most of the available energy E_{avail} ($\sim$50%) is partitioned to product recoil energy, $\langle E_{recoil} \rangle$ (Table 1), with the balance partitioned mostly into the product rotational energy, $\langle E'_{rot} \rangle$, with much less to the product vibrational energy, $\langle E'_{vib} \rangle$. We found that the $E_{avail} \rightarrow E_{internal}$ ($= E'_{rot} + E'_{vib}$) conversion is roughly independent of impact parameter for b up to 1.5 Å, then gradually decreases with increasing b, presumably because at large b collisions there is more energy tied up in orbital motion, which cannot be converted to $E_{internal}$ without violating angular momentum conservation.

2 Dependence on collision orientation. The fact the opacity functions are roughly independent of b (Fig. 5), but significantly less than unity, suggests that there exists a dynamical bottleneck that suppresses reaction, independent of b. The significant increase in the value of $P(b)$ upon excitation of the $C_2H_2^+$ *cis*-bend overtone, implies that the vibrational enhancement might reflect behavior at the bottleneck. To identify the nature of this bottleneck, we will examine correlations between reaction probability and various trajectory geometric parameters at the turning point of the inter-reactant separation. The turning point occurs about 40 fs prior to the actual hydrogen atom transfer event (Fig. 3). Correlations with geometric parameters recorded earlier during the trajectories are discussed below.

Fig. 6 shows a 2-D correlation map of reaction probability for ground state $C_2H_2^+$ versus two different parameters characterizing collision orientation. The definitions of the two parameters are indicated in the schematic of the collision geometry in Fig. 6. $\alpha_{approach}$ is the angle between the acetylene C–C bond and the methane H atom that makes the closest approach to either of the acetylene carbon atoms. This "closest" H atom is the one that is abstracted if the HA reaction occurs. Because the vibrating $C_2H_2^+$ has negligible

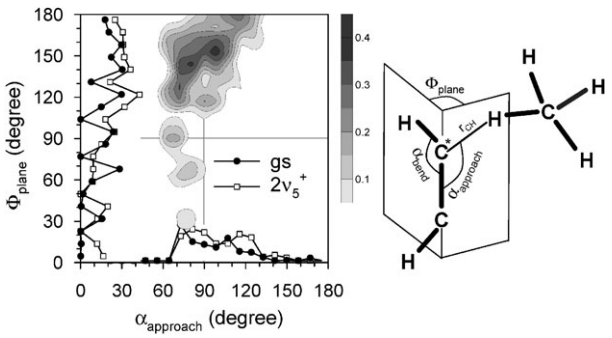

Fig. 6 Dependence of reaction probability on $\alpha_{approach}$ and Φ_{plane}. The contour map is for the ground state only, while the 1-D plots are for both the ground and $2\nu_5^+$ states. The sketch shows the definition of various angles.

chance of being linear at any given point in the trajectory, we define a dihedral angle Φ_{plane} that the "closest" methane H atom makes with respect to the acetylene C–C*–H plane, where C* is the carbon atom being attacked. Φ_{plane} describes whether the acetylene is bending toward ($\Phi_{plane} < 90°$), or away ($\Phi_{plane} > 90°$) from the "closest" methane H atom. Reaction probability is calculated as the fraction of trajectories leading to HA for each range of these two parameters.

The CM turning point is late enough in the trajectory that there is not enough time for significant orientation steering before onset of hydrogen abstraction, but early enough that the collision has not severely perturbed the initial reactant motion. Note that the reaction probability is dominated by collisions where the "closest" H atom of CH_4 approaches acetylene from the side ($\alpha_{approach} = 90° \pm 20°$), and simultaneously the C–C*–H moiety is bent away from the approaching H atom. The probability of having collisions in this range of optimal orientations is $\sim$0.66, but because less than 40% of these collisions actually react, the opacity function $P(b)$ is only $\sim$0.25.

Fig. 6 also gives the uncorrelated one-dimensional curves showing reaction probability *vs.* $\alpha_{approach}$ and Φ_{plane}, for both ground state and for $2\nu_5^+$-excited $C_2H_2^+$. Bending excitation doesn't have any dramatic effect on the shape of the reaction probability curves, *i.e.*, vibrational excitation does not expand the reactive range of either orientation parameter but instead increases the reactivity in favorable orientations. Therefore, we can conclude that while collision orientation controls the overall reactivity, it is not strongly correlated with the vibrational enhancement. Vibrational enhancement must depend on some other aspects of the collisions.

Note that the $\alpha_{approach}$ curves both have a peak at $\alpha_{approach} = 75$–$80°$ that is a consequence of the fact that both acetylene C atoms have similar distance to the abstracted H atom in such geometries, which roughly doubles the probability that the H will be abstracted. The contribution each range of angle makes to the HA cross section depends on the reaction probability *vs.* angle (Fig. 6), but also on the probability of having collisions in a particular orientation (the orientation distribution). The Φ_{plane} orientation distribution is constant, *i.e.*, there is no weighting effect for the dihedral angle. The $\alpha_{approach}$ orientation distribution, however, is proportional to $\sin(\alpha_{approach})$, thus the weighted reaction probability peaks at $\alpha_{approach} = 70$–$100°$.

3 Dependence on $C_2H_2^+$ bend angle. One obvious question, given the strong enhancement from bending excitation, and the fact that the C–C*–H moiety must bend significantly in order to form either the classical or bridging forms of $C_2H_3^+$, is that reactivity might simply be a function of the bend angle at some critical point in the collision. Fig. 7 explores this idea. The angle of interest is the H–C*–C angle (α_{bend} in Fig. 7), where C* is the carbon atom which interacts most strongly with the "closest" methane H atom, *i.e.*, the C atom which abstracts the H atom in reactive collisions. Data is shown for three different sampling times: the beginning of the trajectories, 25 fs before the CM turning point, and right at the turning point. The left column shows the reaction probability for the two reactant states (ground state and $2\nu_5^+$)

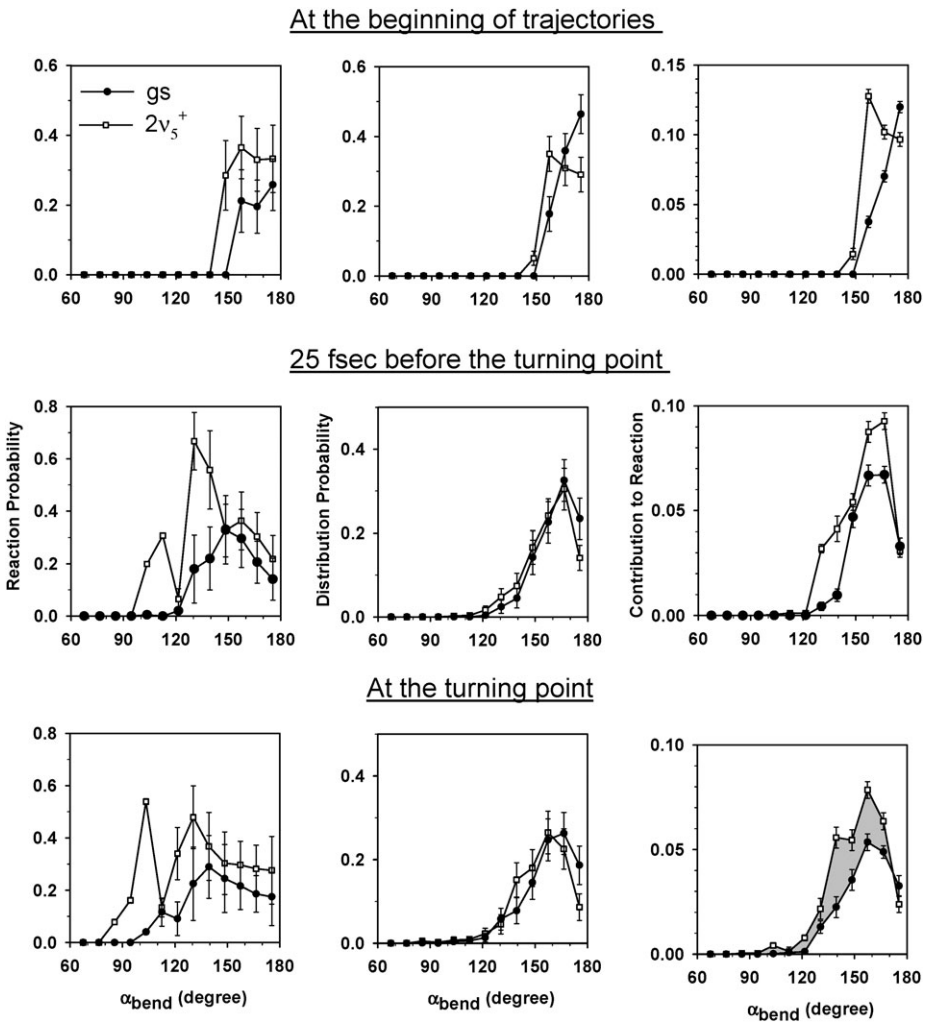

Fig. 7 (Left column) Reaction probability as a function of the value of α_{bend}; (middle column) probability of $C_2H_2^+$ being bent in different ranges of α_{bend}; and (right column) contribution of each α_{bend} range to the HA cross section. In each column, data is shown for both the ground and $2\nu_5^+$ states and for three different sampling times.

as a function of α_{bend}. The center column shows the probability of finding the acetylene with different ranges of bend angle, and the right column is the product of left and center columns. This product represents the contribution of trajectories where acetylene is found in different ranges of bend angle to the total cross section for each state, at the three sampling times.

For geometries sampled at the beginning of the trajectories (top row), several things should be noted. The middle frame shows the range of bend angles explored by the ground state (*i.e.*, zero point level), and the $2\nu_5^+$ state. As expected, the ground state is most likely to be found in near-linear geometry, whereas the $2\nu_5^+$ state is most likely to be found with a α_{bend} near the classical turning point, around 150°. The left frame shows that the $2\nu_5^+$ state is more reactive than the ground state at all ranges of α_{bend}, and that the enhancement factor is independent of α_{bend}, within the uncertainty of the calculations. Of course, we do not expect reactivity to be correlated with the bend angle sampled at the trajectory start, because the collision really starts ~100 fs (several bending vibrational periods) later. The initial vibrational phase is random, therefore, there should be no correlation between the starting angle and the angle when the collision actually begins.

The middle row shows the results sampled 25 fs before the CM turning point, just at the beginning of the strong collisional interaction. Note that by this point, the distributions of bend angle for the two states have become quite similar due to distortion of the $C_2H_2^+$ by the collisional interaction. If reactivity were simply a question of the bend angle at the moment of collision, the similarity of the bend angle distributions would suggest that there should be no significant enhancement from the $2\nu_5^+$ excitation. The left frame shows, however, that the dependence on bend angle of the reaction probabilities for the ground and $2\nu_5^+$ states are, in fact, quite different. The $2\nu_5^+$ state is considerably more reactive than the ground state at bend angles below ~150°, and slightly more reactive at larger angles as well. Taking the product of the left and center frames, the right frame shows that the $2\nu_5^+$ cross section gets larger contributions from all ranges of α_{bend} (except linear) than does the ground state cross section. Note that the difference in reaction probability at

small α_{bend} ($<120^\circ$) has no significant effect on the cross section, because of the low distribution probability of α_{bend} in this range. Instead, it is the higher reaction probability between 120 and 180° that causes the dominant vibrational effect.

The interesting point here is that the reactants still somehow "remember" the initial state of the $C_2H_2^+$ at this point in the trajectories, even though the collisional interaction has distorted the initial bend angle distributions to be almost indistinguishable. This point is even more obvious if the bend angle-reactivity correlation is examined at the CM turning point (Bottom row). The bend angle distributions (middle frame) are very similar for the two states, with only a slight shift to smaller angle for the $2\nu_5^+$ state. Nonetheless, the reaction probability (left frame) is much higher for the $2\nu_5^+$ state at all angles, such that the resulting contributions to the cross section (right frame) are higher for the $2\nu_5^+$ state for all but the point nearest linear geometry.

We also examined the 2-D correlation between the bending angle, α_{bend}, the orientation of the bending plane with respect to the approaching H atom, Φ_{plane}, and the reactivity. In previous systems, this correlation has been illuminating,[23] but here there is no obvious correlation.

4 The precursor complex and its effect on reactivity. As noted in the Introduction, shallow potential wells that might support precursor (*i.e.*, reactant-like) complexes are common in ion–molecule systems, thus the behavior of such complexes is of some interest. Klippenstein proposed a model to rationalize the large mode-specific reactivity enhancements observed for this system, in which it was assumed that the CC stretch vibration remained uncoupled in the weakly-bound precursor complex, whereas the bending vibration coupled to the complex bath modes, and was therefore available to drive reaction. We have suggested precursor mediation to rationalize sharp spikes in cross section at low collision energy,[20,22] and invoked a mode-specific coupling argument reminiscent of Klippenstein's to account for vibrational effects in $PhOH^+ + ND_3$.[15] We have also proposed an alternative scenario whereby precursor-mediated mechanisms might show mode-specific vibrational effects, based on the notion that the probability of trapping into precursor complexes might depend on the reactant vibrational mode.[20] If true, this would rationalize vibrational effects in complex-mediated reaction, without requiring that some modes remain uncoupled in the complexes. Unlike our previous trajectory work, the simulated collision energy in this system is low enough that the precursor-mediated mechanism should still be significant, and indeed, significant numbers of trajectories are observed to form complexes. It should be possible, therefore, to examine the role of the precursor complex and possible connection to the enhancement from $C_2H_2^+$ bending excitation.

Before discussing the trajectory results, we first note that the well depths for the reactant-like complexes (both classical and bridged) calculated at the level of theory used in the trajectories (MP2/6-31+G*) is only ~50% of the well depth calculated at the G3 level, as shown in Fig. 1. As a consequence, we expect that the importance of precursor mechanism will be diminished in the trajectories. The effect should be much as if the trajectories were run at somewhat higher collision energy—a smaller fraction of trajectories will form complexes, and the lifetimes will be reduced. On the other hand, because the interaction between $C_2H_2^+$ and CH_4 in the complexes is weaker than in reality, the coupling of $C_2H_2^+$ vibrational modes to the bath modes should be weaker, making it more likely that they might persist in the complex—a key underpinning of the mode-selective coupling argument.

To identify trajectories that formed complexes, we defined the collision "lifetime" as the time between the first point where the reactant CM separation of the collision partners drops below 3.0 Å, and the point where the separation finally goes above 3.0 Å for the last time (*i.e.*, including any time spent oscillating in and out of 3 Å range). The 3.0 Å trigger distance was chosen as a reasonable estimate of the distance below which there is significant interaction between the partners (Fig. 3). With this definition, direct collisions have lifetimes less than 200 fs, and these account for ~84% of all collisions with $b \leq 3.5$ Å. The rest have a distribution of lifetimes running out to 1400 fs, which is the point where trajectories were terminated. Trajectories with lifetimes greater than 1000 fs all were found to have trapped into the covalently bound $C_3H_6^+$ complex. Some of these dissociate to $C_3H_5^+ + H$, but many remain as $C_3H_6^+$ until terminated, consistent with the large binding energy of this complex, relative to the available energy. The trajectories of interest for probing the mode-selective coupling mechanism are those that form the more weakly bound, short-lived precursor complexes, and these all have collision times between 200 and 1000 fs.

Fig. 8 summarizes the results for all trajectories that formed complexes, including both precursor (11%) and covalent (5%) complexes. The top frame compares the probability of forming complexes for the ground and $2\nu_5^+$ states, as a function of the impact parameter. Probabilities are shown for all complex-forming trajectories, and also for the precursor-only subset. The probability is quite high for collisions at small impact parameters, reflecting the fact that such intimate collisions are likely to be quite inelastic, with enough translational-to-internal ($T \rightarrow V, R$) energy transfer to trap the partners in the weak precursor wells. Above ~2 Å impact parameter, the probability of trapping into a complex diminishes rapidly, because the strong interactions needed to drive $T \rightarrow V, R$ transfer become increasingly unlikely in less central collisions. Note that there is a slightly higher probability of trapping into a complex if the $C_2H_2^+$ has bending excitation. On the other hand, there is no obvious effect from the CC stretch excitation (not shown in the figure).

The middle frame shows the probability that the complexes decay to HA products. Again, probabilities are shown for all complex-forming trajectories, and also for the precursor-only subset of the trajectories. The *b*-weighted branching of "all complexes" to HA products is 20–25%, with a slightly higher HA branching for complexes formed by bending-excited $C_2H_2^+$. If only the precursor complexes are examined, the branching to HA products increases to 30–40%, again with the probability enhanced by the bending excitation, but not by the CC stretch (not shown). The other main channel in

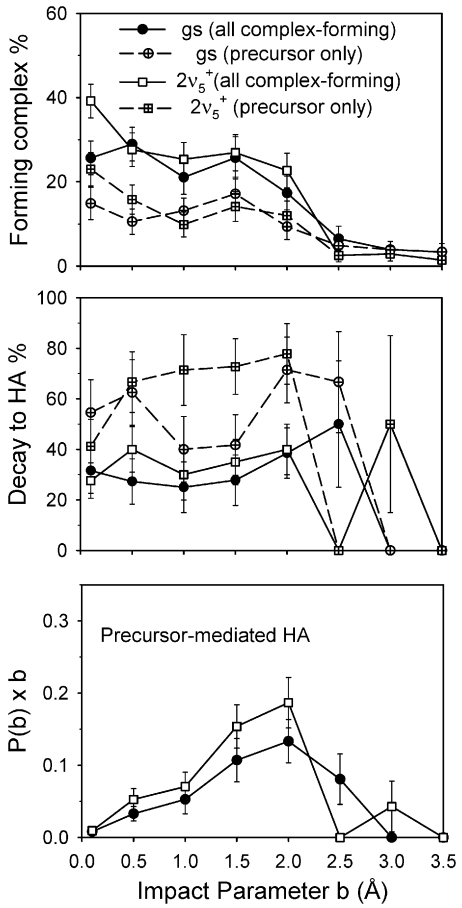

Fig. 8 (Top) Probability for all complex-forming trajectories, and for the precursor-only subset *vs.* impact parameter, for different vibrational states; (middle) probability for decay of all complexes and precursor complex to HA products *vs.* impact parameter, for the ground and $2\nu_5^+$ states; and (bottom) precursor-mediated HA opacity functions (*b*-weighted) for different vibrational states.

decay of the complex is dissociation back to reactants. Decay *via* TS2 (Fig. 1) to form $C_3H_{6-x}^+$ is also observed (5% branching), however, in that case the collision time is >1000 fs, and these trajectories are counted with those that form $C_3H_6^+$. Note also that the reason that the HA branching probability for "all complexes" is lower than for precursor complexes is that the $C_3H_6^+$ complexes decay almost exclusively to $C_3H_{6-x}^+$ products.

The bottom frame shows the *b*-weighed product of the top and middle frames, corresponding to the contributions of precursor-mediated trajectories to the HA cross section, as a function of impact parameters. Because of the *b*-weighing, the largest contribution is from trajectories in the range around 1.5–2 Å, and bend excitation of the $C_2H_2^+$ reactant increases the contribution over most of the range of *b*. The total contribution of the precursor mechanism to the total HA cross section is gotten by summing over *b* (eqn (1)), with the result that the precursor mechanism is, indeed, enhanced by bending excitation (partial HA cross section = 1.28 Å^2, 1.22 Å^2 and 1.45 Å^2 for the ground, ν_2^+, and $2\nu_5^+$ states, respectively). Most of the enhancement by $2\nu_5^+$ comes from the higher branching to HA, of complexes formed from bend-excited $C_2H_2^+$, suggesting that there is some validity to the scenario previously proposed to rationalize mode effects in a precursor mechanism. Note, however, that this enhancement ($\sim$13%) is actually smaller than the $\sim$55% enhancement (Table 1) of the total HA cross section. The dominant enhancement by the bending excitation, therefore, comes from direct collisions, and if we subtract the precursor-mediated contribution, we find that the direct mechanism is enhanced by $\sim$63%. It is interesting to note that the enhancement by the CC stretch, while small, completely comes from the direct collisions.

We also looked for evidence of mode-selective or weak coupling of the $C_2H_2^+$ vibrations with the bath modes of the complex. It turns out that in most precursor-mediated trajectories, there is repeated H-transfer back and forth between the collision partners, and of course this repeated bond breaking/formation is accompanied by large changes in the nature of the vibrations, such that all reactant modes are strongly coupled. In fact, the dominant route for trapping into the precursor seems to a frustrated direct HA reaction, *i.e.*, the collision starts with direct H atom transfer, but in some collisions there is so much accompanying $T \rightarrow V$ transfer that the products cannot separate, and trap into a complex.

The equilibrium structure of both classical and bridged precursor complexes is reactant-like (*i.e.*, $C_2H_2^+$–CH_4). Attempts to optimize structures for product-like complexes (*i.e.*, $C_2H_3^+$–CH_3) converged to $C_2H_2^+$–CH_4. Nonetheless, in the complexes explored by the trajectories, the H atom transferred repeatedly and the system was observed to spend roughly equal time in $C_2H_2^+$–CH_4 and $C_2H_3^+$–CH_3 geometries. This propensity for the higher energy $C_2H_3^+$–CH_3 structure is a density-of-states effect, driven by the larger number of low frequency vibrations for the less symmetric $C_2H_3^+$–CH_3 species. The same effect is seen in the dissociation from the precursor complex, where both RRKM and trajectories see 60% branching to HA products, despite the energy for decay back to reactants being significantly lower.

5 The feasibility of devising Polanyi-type rules for polyatomic reactions. Polanyi and co-workers[40] carried out a series of model studies comparing the relative effectiveness of vibrational and collision energy in driving reaction over a barrier for a triatomic A + BC system. It was shown that for early barrier reactions, *i.e.*, potential energy surfaces (PES) with a barrier in the entrance channel, collision energy is most effective in driving reaction, because this adds momentum to the coordinate that is perpendicular to the barrier. For late barrier reactions, conversely, vibrational excitation is more effective, because this adds momentum that helps carry the system "around the bend" in the PES, and over the barrier. In the discussion above, we argue that it is primarily the momentum associated with the bending vibration, rather than the geometrical distortion, that is responsible for the observed vibrational effects. Furthermore, it was shown that the collisions responsible for the enhancement are direct, with only a single turning point in the motion of the centers of mass of the collision partners. These observations raise the question of whether such

reactions can be simplified somehow to resemble the simpler A + BC systems Polanyi described, and whether such simplication could be made predictive.

In a previous study of the HA reaction of H_2CO^+ with methane,[31] we were able to devise a reduced PES, and when reactive and non-reactive trajectories were projected on this PES, they closely resembled the sort of vibrational momentum-driven barrier crossing behind the Polanyi rules. In particular, momentum in the CH_4 umbrella distortion coordinate, with the proper phase, would push the system through a bottleneck, into the product well, while collision energy largely resulted in reflection from the repulsive wall, with no reaction. The PES simplification process was guided by the trajectory results, which showed reaction only for approach in narrow ranges of several reactant orientation parameters (analogous to $\alpha_{approach}$ and Φ_{plane} in this system), which could, therefore, be frozen in the PES reduction process. Furthermore, coordinates such as rotation of methane about the H*–CH_3 axis, where H* is the atom being abstracted, and distortion of the methyl group from C_{3v} symmetry, have little effect on the bottleneck and therefore could also be frozen.

The $C_2H_2^+$ + CH_4 system is somewhat less constrained, however, as shown in Fig. 6 reaction also only occurs for certain ranges of $\alpha_{approach}$ and Φ_{plane}, and there is no reason to expect that HA would be particularly sensitive to rotation or distortion of the methyl group. Therefore, we followed a similar procedure to reduce the 21-dimensional PES to a 2-D PES, shown in Fig. 9. In Fig. 9, r_{CH} is the distance between the acetylene C atom being attacked and the ''closest'' methane H atom. For the HA reaction, r_{CH} correspond to the reactant approach coordinate. α_{bend} directly correlates with the $2\nu_5^+$ excitation, and for a reactive trajectory, α_{bend} describes the transition from reactants to products, because the C–C*–H angle bends going from $C_2H_2^+$ to $C_2H_3^+$. This reduced surface was fit to 1100 points calculated at the MP2/6-31+G* level of theory. As in the previous study, we froze the CH_3 moiety in C_{3v} symmetry and $\alpha_{approach}$ at 100°, and optimized all other coordinates at each point on the surface. On this reduced surface, there are two wells corresponding to products. One, with $r_{CH} \sim 1.4$ Å and $\alpha_{bend} \sim 135°$, corresponds to the classical form of $C_2H_3^+$, and the second, at $r_{CH} \sim 1.6$ Å and $\alpha_{bend} \sim 165°$, corresponds to the bridged form. On the full PES, there is no barrier in excess of the reactant energy for the HA reaction, however, on this reduced surface, which is constrained in the orientation found to be most reactive at 0.5 eV, there is a saddle point about 0.25 eV above the entrance well. This barrier corresponds to the energy required to distort and rehybridize the $C_2H_2^+$ reactant, to allow formation of the classical structure of the $C_2H_3^+$ product. Note that there is no barrier, even on the reduced surface, to formation of the bridged structure, however, almost no trajectories were observed to directly form the bridged structure, because this process requires very symmetric collision geometries.

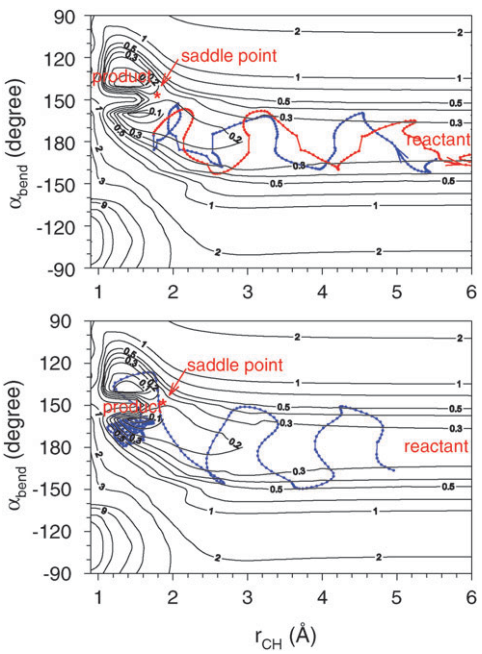

Fig. 9 Reduced potential energy surface for $C_2H_2^+$ + CH_4 → $C_2H_3^+$ + CH_3 calculated at the MP2/6-31+G* level. The contour labels are the potential energy relative to the reactants. The dotted lines in the top and bottom frames, respectively, show a non-reactive trajectory with ground state $C_2H_2^+$, and a reactive trajectories with $2\nu_5^+$-excited $C_2H_2^+$.

The reduced surface shown in Fig. 9 resembles a late-barrier surface of the type that, as Polanyi rules suggest, should be enhanced by excitation of the vibration that corresponds to the transverse motion in the entrance channel. This motion corresponds to $C_2H_2^+$ bending, which is found to strongly enhance reaction. The top frame of the figure projects a typical non-reactive trajectory with collision energy of 0.5 eV and reactant ZPE. The system has sufficient translational energy to overcome the barrier on the reduced surface, however, no reaction is observed. The lower frame shows the projection of a typical reactive trajectory with $2\nu_5^+$ excitation. The momentum in the bending motion carries the system over the barrier to form the classical structure of the $C_2H_3^+$ + CH_3 products, which immediately isomerize to the more stable bridged form, where the trajectory remains until terminated.

We conclude that for systems where the range of reactive orientations is sufficiently constrained, it is possible to construct a reduced PES (or perhaps a family of reduced PESs) that provide a natural way to rationalize the effects of different types of reactant motion on scattering/reactivity.

V. Conclusions

Quasi-classical trajectories calculated at the MP2/6-31+G* level of theory are able to reproduce the large vibrational effects of $C_2H_2^+$ *cis*-bending for hydrogen abstraction in $C_2H_2^+$ + CH_4. Analysis of the trajectories shows that the bending effect is not simply a consequence of enhanced reactivity in bent geometries, but rather, the excitation of the bending motion adds momentum along the reaction coordinate. Similar effects might be expected in other polyatomic systems, particularly at collision energies where the collision interaction and vibration have similar time scales.

Acknowledgements

J.L. acknowledges the donors of the American Chemical Society Petroleum Research Fund (PRF #48208-G6), CUNY Collaborative Grant and PSC-CUNY award for support of this work. S.L.A. acknowledges support by National Science Foundation (CHE-0647124). We thank William Hase (Texas Tech) for providing VENUS99, and Theresa Windus (Iowa State) for helpful discussions regarding convergence issues.

References

1 S. Wexler and N. Jesse, *J. Am. Chem. Soc*., 1962, **84**, 3425–3432.
2 F. H. Field and M. S. B. Munson, *J. Am. Chem. Soc*., 1965, **87**, 3289–3294.
3 F. P. Abramson and J. H. Futrell, *J. Chem. Phys*., 1966, **45**, 1925–1931.
4 J. J. Myher and A. G. Harrison, *Can. J. Chem*., 1968, **46**, 1755–1762.
5 A. A. Herod and A. G. Harrison, *Int. J. Mass Spectrom. Ion Phys*., 1970, **4**, 415–431.
6 N. G. Adams and D. Smith, *Chem. Phys. Lett*., 1977, **47**, 383–387.
7 J. K. Kim, V. G. Anicich and J. W. T. Huntress, *J. Phys. Chem*., 1977, **81**, 1798–1805.
8 K. Honma, I. Koyano and I. Tanaka, *Bull. Chem. Soc. Jpn*., 1978, **51**, 1923–1926.
9 T. M. Orlando, B. Yang and S. L. Anderson, *J. Chem. Phys*., 1989, **90**, 1577–1587.
10 Y.-H. Chiu, H. Fu, J.-T. Huang and S. L. Anderson, *J. Chem. Phys*., 1994, **101**, 5410–5412.
11 Metayer-Zeitoun, C. Alcarez, S. L. Anderson, H. Palm and O. Dutuit, *J. Phys. Chem*., 1995, **99**, 15523–15531.
12 Y.-H. Chiu, H. Fu, J.-T. Huang and S. L. Anderson, *J. Chem. Phys*., 1995, **102**, 1199–1216.
13 S. J. Klippenstein, *J. Chem. Phys*., 1996, **104**, 5437–5445.
14 Q. Cui, Z. Liu and K. Morokuma, *J. Chem. Phys*., 1998, **109**, 56–62.
15 R. J. Green, H.-T. Kim, J. Qian and S. L. Anderson, *J. Chem. Phys*., 2000, **113**, 4158–4170.
16 S. G. Lias, in *NIST Standard Reference Database Number 69*, ed. P. J. Linstrom and W. G. Mallard, National Institute of Standards and Technology, Gaithersburg, MD, 2003, http://webbook.nist.gov.
17 S. G. Lias, J. E. Bartmess, J. F. Liebman, J. L. Holmes, R. D. Levin and W. G. Mallard, *J. Phys. Chem. Ref. Data*, 1988, **17**, 1–796.
18 M. T. Rodgers, K. M. Ervin and P. B. Armentrout, *J. Chem. Phys*., 1997, **106**, 4499–4508.
19 J. Liu, B. V. Devener and S. L. Anderson, *J. Chem. Phys*., 2002, **117**, 8292–8307.
20 J. Liu, B. V. Devener and S. L. Anderson, *J. Chem. Phys*., 2003, **119**, 200–214.
21 J. Liu and S. L. Anderson, *Int. J. Mass Spectrom*., 2005, **241**, 173–184.
22 J. M. Boyle, B. W. Uselman, J. Liu and S. L. Anderson, *J. Chem. Phys*., 2008, **128**, 114304.
23 J. M. Boyle, J. Liu and S. L. Anderson, *J. Phys. Chem. A*, 2009, **113**, 3911–3921.
24 W. L. Hase, K. Bolton, P. de Sainte Claire, R. J. Duchovic, X. Hu, A. Komornicki, G. Li, K. Lim, D. Lu, G. H. Peslherbe, K. Song, K. N. Swamy, S. R. Vande Linde, A. Varandas, H. Wang and R. J. Wolf, *VENUS99: A General Chemical Dynamics Computer Program*, 1999.
25 V. Bakken, J. M. Millam and H. B. Schlegel, *J. Chem. Phys*., 1999, **111**, 8773–8777.
26 J. Frisch, G. W. Trucks, H. B. Schlegel, G. E. Scuseria, M. A. Robb, J. R. Cheeseman, J. A. Montgomery, T. V. Jr, K. N. Kudin, J. C. Burant, J. M. Millam, S. S. Iyengar, J. Tomasi, V. Barone, B. Mennucci, M. Cossi, G. Scalmani, N. Rega, G. A. Petersson, H. Nakatsuji, M. Hada, M. Ehara, K. Toyota, R. Fukuda, J. Hasegawa, M. Ishida, T. Nakajima, Y. Honda, O. Kitao, H. Nakai, M. Klene, X. Li, J. E. Knox, H. P. Hratchian, J. B. Cross, C. Adamo, J. Jaramillo, R. Gomperts, R. E. Stratmann, O. Yazyev, A. J. Austin, R. Cammi, C. Pomelli, J. W. Ochterski, P. Y. Ayala, K. Morokuma, G. A. Voth, P. Salvador, J. J. Dannenberg, V. G. Zakrzewski, S. Dapprich, A. D. Daniels, M. C. Strain, O. Farkas, D. K. Malick, A. D. Rabuck, K. Raghavachari, J. B. Foresman, J. V. Ortiz, Q. Cui, A. G. Baboul, S. Clifford, J. Cioslowski, B. B. Stefanov, G. Liu, A. Liashenko, P. Piskorz, I. Komaromi, R. L. Martin, D. J. Fox, T. Keith, M. A. Al-Laham, C. Y. Peng, A. Nanayakkara, M. Challacombe, P. M. W. Gill, B. Johnson, W. Chen, M. W. Wong, C. Gonzalez and J. A. Pople, *GAUSSIAN 03 (Revision C.01)*, Gaussian, Inc., Wallingford, CT, 2004.
27 G. B. Bacskay, *Chem. Phys*., 1981, **61**, 385–404.
28 J. Liu, B. W. Uselman, J. M. Boyle and S. L. Anderson, *J. Chem. Phys*., 2006, **125**, 133115.
29 L. Laaksonen, gOpenMol, available at http://www.csc.fi/gopenmol/, Espoo, Finland, 2.2 edn, 2002.
30 J. Liu, K. Song, W. L. Hase and S. L. Anderson, *J. Chem. Phys*., 2003, **119**, 3040–3050.
31 J. Liu, K. Song, W. L. Hase and S. L. Anderson, *J. Am. Chem. Soc*., 2004, **126**, 8602–8603.
32 J. Liu, K. Song, W. L. Hase and S. L. Anderson, *J. Phys. Chem. A*, 2005, **109**, 11376–11384.
33 J. Liu, B. van Devener and S. L. Anderson, *J. Chem. Phys*., 2004, **121**, 11746–11759.
34 W. H. Miller, W. L. Hase and C. L. Darling, *J. Chem. Phys*., 1989, **91**, 2863–2868.
35 A. Untch, R. Schinke, R. Cotting and J. R. Huber, *J. Chem. Phys*., 1993, **99**, 9553–9566.
36 W. H. Press, S. A. Teukolsky, W. T. Vetterling and B. P. Flannery, *Numerical Recipes in C. The Art of Scientific Computing*, Cambridge University Press, Cambridge, UK, 1992.
37 H.-T. Kim, J. Liu and S. L. Anderson, *J. Chem. Phys*., 2001, **115**, 5843–5858.
38 J. Liu, B. Van Devener and S. L. Anderson, *J. Chem. Phys*., 2005, **123**, 204313.
39 R. D. Levine and R. B. Bernstein, *Molecular Reaction Dynamics and Chemical Reactivity*, Oxford University Press, New York, 1987.
40 J. C. Polanyi and W. H. Wong, *J. Chem. Phys*., 1969, **51**, 1439–1450.

